Scientia Iranica (2024) 31(4), 330–345

Sharif University of Technology
Scientia Iranica
Transactions B: Mechanical Engineering
https://scientiairanica.sharif.edu

Conceptual modeling and parametric study of the nonlinear dynamics of the floating wind turbine in the presence of primary and internal resonance

S. Ghabraei, H. Moradi*, and Gh. Vossoughi

Department of Mechanical Engineering, Sharif University of Technology, Tehran, P.O. Box 11155-9567, Iran.

Received 16 July 2022; received in revised form 2 February 2023; accepted 5 April 2023

KEYWORDS
Floating wind turbine;
Tension leg platform;
Surge degree of freedom;
Fore-aft degree of freedom;
Wind and wave loading;
Nonlinear dynamics;
Perturbation;
Primary and internal resonance.

Abstract. In this paper, a conceptual model is proposed to investigate the nonlinear dynamics of the transverse vibrations of the floating wind turbine. The conceptual models are the best tools to capture the most important phenomena in the dynamic response of the systems. First, the surge dynamics of the Tension Leg Platforms (TLP) is modeled as a nonlinear spring. Then, the fore-aft motions of the wind turbine are modeled as a spring-mass system. Then, simulations are carried out to evaluate the time response of the proposed model. Afterward, the FAST code is utilized to verify the proposed model. The internal resonance and its combinations with the primary resonance are studied by the multiple time scale method. Finally, the frequency response curve is obtained, and the effect of the various parameters of the system on the amplitude and the stability of the oscillations are investigated.

1. Introduction

Due to the damaging effects of fossil fuels on the environment, such as global warming and pollution, developing technologies to exploit renewable energies is essential nowadays to fulfill the required electrical energy. Among the renewable energy sources, wind energy is one of the fastest-growing. For example, now wind energy is the main source of renewable power in the United States. Conventional wind turbines are horizontal-axis, three-bladed wind turbines that generate electricity by converting the mechanical energy of the wind to the rotation of the blades and, consequently, the rotation of the shaft of the generator. According to where the turbine is implemented, the wind turbines are categorized as offshore or onshore

*. *Corresponding author. Tel.: +98 21 66165545; Fax: +98 21 66000021*
E-mail address: hamedmoradi@sharif.edu (H. Moradi)

To cite this article:
S. Ghabraei, H. Moradi, and Gh. Vossoughi, "Conceptual modeling and parametric study of the nonlinear dynamics of the floating wind turbine in the presence of primary and internal resonance,
Scientia Iranica (2024) **31**(4), pp. 330-345
DOI: 10.24200/sci.2023.60580.6883

wind turbines. In the same manner, according to the type of platform on which the wind turbine is installed, the offshore wind turbines could be categorized as bottom fixed or Floating Offshore Wind Turbines (FOWT). In offshore areas, the wind blows with higher speed and more reliability, which promises more reliable electricity generation. Unfortunately, the cost of the implantation of the bottom fixed platforms (e.g., jacket and monopole) increases significantly for the offshore areas with a depth of 50 m and more. Therefore, floating platforms such as the Spar, Semi-submersible, and Tension Leg Platforms (TLP) are practical solutions for offshore wind electricity generation in these areas. However, the floating platforms are more complex than the fixed bottom platforms as well as have many challenging technical difficulties [1].

The floating foundations demonstrate more complexity than the fixed bottom platforms due to the low stiffness and damping of the floating platform. Floating platform motions increase the high cycle fatigue failures in the structure of the wind turbine. Moreover, the coupling between the floating platforms and the wind turbine tower increases the complexity of the system and may result in instability. In order to design the floating wind turbine with satisfying reliability, the dynamic of the whole system, in case of idling and operational conditions, should be studied. In the idling condition, the absence of significant damping may lead to structural instabilities. Also, in operational conditions, the amplitude and frequency of the external excitations of the wave and wind may lead to instability [2].

Among the designed floating platforms, TLP merit more robustness and lower fatigue loads. Therefore, the TLP may be the most appropriate floating platform for the installation of huge multi-megawatt wind turbines in offshore areas [3].

The TLP was first designed for the exploitation of oil and gas resources in deep offshore areas. The tension platform includes a semi-submerged structure, on which the facilities will be installed, and pretensioned tendons, which provide stability for the structure. The tendons are expensive and prone to fatigue or large amplitude vibrations, which are due to the wave loadings. The appropriate dynamic model of a system is the cornerstone of studying any system. Therefore, due to the complexity of the TLP, worthy research has been done to study the dynamics of the TLP. Among them, the coupling behavior of various degrees of freedom and different nonlinearities in the response of the TLP have been studied [4]. Moreover, implementing the energy balance method to derive a nonlinear stiffness matrix for the TLP [5], investigation of TLP behavior under tendon damage [6], and numerical and physical modeling of a TLP for offshore wind turbines [7] have been carried out.

The natural frequency of the surge, sway, and yaw directions is much less than the one in the heave, roll, and pitch directions due to the tendon's geometrical stiffness [5]. Therefore, surge, sway, and yaw directions are susceptible to large amplitude vibrations due to the wind and wave loadings. Consequently, many efforts have been dedicated to studying the dynamics of the TLP. In this regard, analyses of the response of the TLP with a hydro-pneumatic tensioner [8] and the coupled surge and heave dynamics of the TLP [9] have been carried out. However, the complexity of the floating wind turbine is considerably more than that of a single TLP due to the various wind and wave loading and interactions between the floating platform and the wind turbine. In this regard, the development of a comprehensive simulation tool for modeling the coupled dynamic response of FOWT [10], numerical assessment of a TLP wind turbine in intermediate water [11], numerical and experimental study on the effect of the tuned mass dampers on the dynamic response of the TLP [12], computations and measurements of the global drag force on a TLP [13], investigation of the effect of the added mass fluctuation and lateral vibration absorbers on the vertical nonlinear vibrations of the offshore wind turbine [14] and model development and uniform energy extraction of an FOWT [15] have been done.

FAST, developed by the National Renewable Energy Laboratory (NREL) [16], is a well-known and validated numerical simulator for FOWTs. Many efforts have been carried out to validate the FAST code. In this regard, validation has been conducted for a FAST spar-type floating wind turbine numerical model using basin test data [17], and a code comparison has been performed for an NREL-FAST model of the Levenmouth Wind Turbine against the GH Bladed commissioning results [18]. In addition, many researchers used the FAST as a validation tool. For example, a critical analysis of the technical implications of upscaling the offshore wind turbine, focusing on aero-hydro-servo-elastic design [19], used the FAST as a validation tool.

In most engineering systems, vibrations have adverse consequences, such as the reduction of the reliability of the system, amplification of the fatigue loads, etc. Moreover, phenomena such as resonance may lead to the collapse of the structure in a few seconds. Therefore, analytical approaches have been used to study the vibrations in many challenging engineering problems [20,21]. The large amplitude motions of the floating platform exceed the fatigue loads on the floating platform tendons, tower of the wind turbine, and wind turbine blades as well [22,23]. Moreover, the installation of a large multi-megawatt wind turbine increases the complexity of the system vibrations [3,19,24].

Motivated by the above literature review, in this paper, longitudinal vibrations of the FOWT, consisting of the surge motions of the floating platform and the fore-aft motions of the wind turbine tower, as well as the coupling between them, are investigated. In this regard, the NREL 5 MW wind turbine coupled with MIT/NREL TLP is considered for the analysis [25]. To study the coupled longitudinal vibrations of the FOWT, a simple conceptual model is presented. The conceptual models provide a comprehensive view of the dominant dynamics of a system without mathematical complexities. In this regard, first, the equivalent stiffness of the surge vibrations of the MIT/NREL TLP floating platform is calculated. Then, the equivalent fore-aft stiffness of the NREL 5 MW wind turbine, according to the tower tip displacements, is derived. Afterward, the proposed model is validated via the comparison of the simulation results with those of the FAST. Then, the nonlinear dynamics of the FOWT are studied using the method of Multiple Time Scales (MTS). According to the approximate solution obtained by the method of MTS, energy transfer between the tower and floating platform (internal resonance) and its combination with primary resonance due to the wave and wind loadings have been studied. In this regard, the effects of wave and wind loading amplitude and frequency, TLP floating equivalent damping, and TLP floating platform equivalent nonlinear stiffness on vibration amplitude and stability are investigated. This analysis is conducted by plotting frequency response curves obtained from the closed-form solution. Through the frequency response curves, nonlinear phenomena such as jumps, bifurcations, and unstable steady oscillations have been observed. Studying the energy transfer between the tower and the floating platform helps to design passive vibration absorbers for the FOWT. In this paper, a procedure for studying the aforementioned nonlinear phenomena in the FOWT is introduced and followed, which could be used in the design of the FOWT, which is the main distinguishing difference between this paper and the previously done research.

2. Nonlinear bulk modeling of the surge motions of the floating wind turbine

A schematic of a floating wind turbine with a TLP is shown in Figure 1. The submersible part of the platform is connected to the seabed by means of the pretensioned tendons. The submersible's buoyancy is greater than its weight; therefore, the tendons are in tension. Preloaded tendons are the main source of TLP stability. As aforementioned, the displacement of the platform in the heave direction is significantly smaller than the one in the surge direction. Therefore, the heave displacement is neglected for the sake of simplicity. The general properties of the NREL 5 MW wind turbine and NREL/MIT TLP are represented in Tables 1 and 2, respectively.

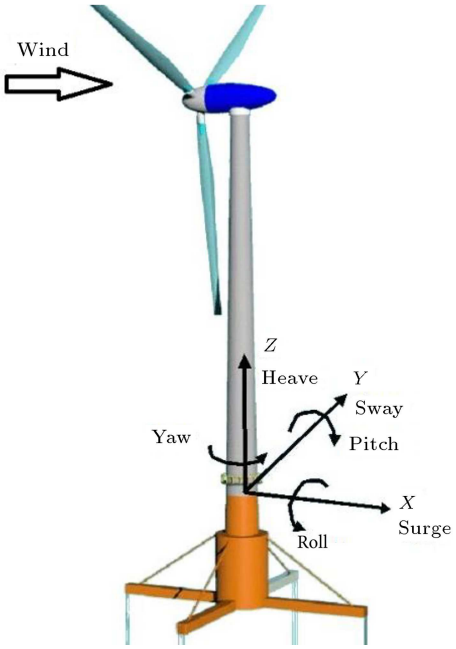

Figure 1. Schematic of the floating wind turbine with TLP [26].

2.1. Equations of the motion of the floating wind turbine

The surge motions of the floating platform and the fore-aft vibrations of the wind turbine tower are mostly due to the transverse wave and wind loading. In order to capture the dominant phenomena and for the sake of simplicity, it is rational to reduce the transverse longitudinal motions of the floating wind turbine, as shown in Figure 2, to a reduced bulk model, as depicted in Figure 3. Coefficient K_1 is the equivalent surge stiffness of the floating platform, d_1 is the equivalent damping coefficient of the platform due to interaction with seawater, K_2 is the equivalent fore-aft stiffness of the wind turbine tower, d_2 is the damping coefficient of the wind turbine tower due to the interaction of the blades, M_1 is the mass of the platform, M_{added} represents the hydrodynamics added mass, and M_2 is the mass of the nacelle and the rotor altogether. According to the location of the tower center of mass, the mass of the tower is added as a concentrated mass to the mass of the platform and the mass of the nacelle in order to increase the model's accuracy. Finally, the governing equations of the motion of the transverse vibrations of the floating wind turbine could be written as:

$$\left(M_1 + 0.56M_{tower} + M_{added}\right)\ddot{u}_1 + K_1u_1 - K_2u_2 + d_1\dot{u}_1 = F_{wave},$$

Table 1. Summary of properties of the NREL 5 MW baseline wind turbine.

Rating (MW)	5
Rotor orientation, configuration	Upwind, 3 blades
Control	Variable speed, collective pitch
Drive train	High speed, multiple-stage gearbox
Rotor, hub diameter (m)	126, 3
Hub height (m)	90
Cut-in, rated, cut-out wind speed (m s^{-1})	3, 11.4, 25
Rotor mass (kg)	110,000
Nacelle mass (kg)	240, 000
Tower mass (kg)	347, 460
Height of the tower center of mass (m)	38.23
Location of overall center of mass of the WT	0.2 m upwind of tower centerline, 64.0 m above Still Water Level (SWL)
First tower fore-aft natural frequency	0.32 (Hz)
structural damping ratio	0.1%

Table 2. Summary of properties of the MIT/NREL floating platforms.

Diameter or width × length (m)	18
Draft (m)	47.89
Mass (kg)	8600000
CM location of the platform below SWL (m)	40.61
Number of mooring lines	8 (4pairs)
Depth to fairleads, anchors (m)	47.89, 200
Radius to fairleads, anchors (m)	27, 27
Unstretched line length (m)	151.7
Line extensional stiffness (N)	1,500,000,000
Platform added mass in the surge direction (kg)	9E+6 kg

$$\left(M_2 + 0.44M_{tower}\right)\ddot{u}_2 + K_2 u_2 - K_2 u_1 + d_2\dot{u}_2 = F_{wind}. \quad (1)$$

2.2. Equivalent surge stiffness of the platform in FOWT

The stiffness matrix for the transverse vibrations is obtained for arbitrary u_1 and u_2 displacements. Regarding u_1, which represents displacement in surge degree of freedom, the equilibrium equation in surge direction could be written as:

$$K_1 u_1 = 4\left(T_0 + \Delta T\right)\sin\theta, \quad (2)$$

where K_1 is the equivalent stiffness in the surge direction, T_0 is the pretension in tendons, θ is the inclination angle of tendons due to the surge displacements, and ΔT is the increase in tension force in tendons due to the displacements. The increase in tendon tension could be calculated as follows:

$$\Delta T = \left(\sqrt{u_1^2 + L^2} - L\right),$$

$$K_0 = \left(\sqrt{\left(\frac{u_1}{L}\right)^2 + 1} - 1\right) LK_0, \quad (3)$$

where $K_0 = \frac{AE}{L}$ is the extensional stiffness of the tendons. By using Taylor expansion, the above equation

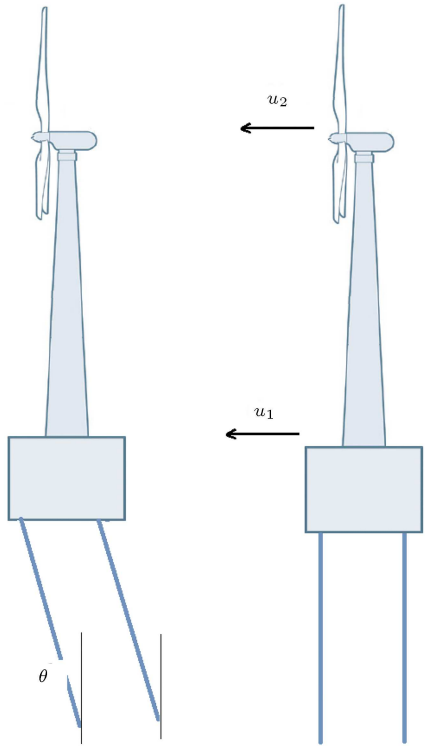

Figure 2. Schematic of the floating wind turbine.

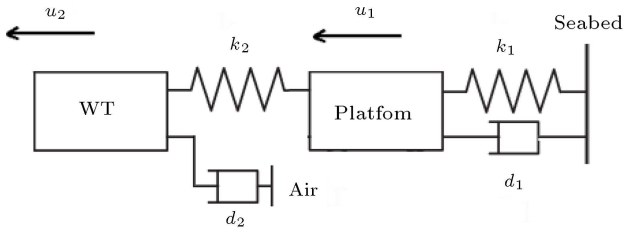

Figure 3. Schematic of the proposed conceptual model.

can be simplified as:

$$\left(\frac{1}{2}\left(\frac{u_1}{L}\right)^2+1-1\right)LK_0=\frac{1}{2}\left(\frac{u_1}{L}\right)^2LK_0. \tag{4}$$

Therefore, the equivalent stiffness of the surge degree of freedom could be written as:

$$K_1=4\left(\frac{T_0}{L}+\frac{AE}{2L^3}x^2\right). \tag{5}$$

By substitution of Eqs. (1) and (2), the governing equation of motion could be written as:

$$\begin{aligned}&\left(M_1+0.56M_{tower}+M_{added}\right)\ddot{u}_1\\&\quad+K_{11}u_1+K_{12}u_1^3-K_2u_2+d_1\dot{u}_1=F_{wave},\\&\left(M_2+0.44M_{tower}\right)\ddot{u}_2\\&\quad+K_2u_2-K_2u_1+d_2\dot{u}_2=F_{wind}.\end{aligned} \tag{6}$$

The coefficient behind the M_{tower} in the above equation is obtained through the optimizations.

Finally, Eq. (6) is rewritten as follows:

$$\begin{aligned}&\ddot{u}_1+s_{11}u_1+s_{12}u_1^3-s_2u_2+b_1\dot{u}_1=f_{wave},\\&\ddot{u}_2+\tilde{s}_2u_2-\tilde{s}_2u_1+b_2\dot{u}_2=f_{wind},\end{aligned} \tag{7}$$

where:

$$s_{11}=\frac{K_{11}}{M_1+0.56M_{tower}+M_{added}},$$

$$s_{12}=\frac{K_{12}}{M_1+0.56M_{tower}+M_{added}},$$

$$s_2=\frac{K_2}{M_1+0.56M_{tower}+M_{added}},$$

$$b_1=\frac{d_1}{M_1+0.56M_{tower}+M_{added}},$$

$$\tilde{s}_2=\frac{K_2}{M_2+0.44M_{tower}},$$

$$b_2=\frac{d_2}{M_2+0.44M_{tower}},$$

$$f_{wind}=\frac{F_{wind}}{M_2+0.44M_{tower}},$$

and

$$f_{wave}=\frac{F_{wave}}{M_1+0.56M_{tower}+M_{added}}.$$

In order to assess the equivalent stiffness in the direction of the u_2 degree of freedom, considering the geometrical properties of the tower of the wind turbine, wind turbine tower is considered as a cantilever beam with the variable cross sectional properties; as defined in the Table 3. Then, the deflection of the tip of the wind turbine tower is calculated under a 1 N transverse force. In order to calculate the equivalent fore-aft stiffness of the WT tower, Eq. (8) obtained as shown in Box I.

In Eq. (8), the L_t is the length of the wind turbine tower. The integration origin in the above equation is the tip of the tower where $x=0$.

2.3. Simulation of the model and its validation

In this section, to validate the proposed governing equations for the transverse vibrations of the floating wind turbine, the time history of the motions in the surge and the fore-aft degrees of freedom are obtained. Then, to validate the model, the obtained results are compared with the FAST code V8.0 ones. For this purpose, the corresponding parameters of Eq. (7) is calculated according to Tables 1, 2, and 3 as s_{11}=0.0116,

Table 3. Distributed tower properties of the NREL 5 MW wind turbine [27].

Elevation (m)	Mass density (kg/m)	Tower fore-aft stiffness (N.m^2)
0.00	5590.87	614.34E+9
8.76	5232.43	534.82E+9
17.52	4885.76	463.27E+9
26.28	4550.87	399.13E+9
35.04	4227.75	341.88E+9
43.80	3916.41	291.01E+9
52.56	3616.83	246.03E+9
61.32	3329.03	206.46E+9
70.08	3053.01	171.85E+9
78.84	2788.75	141.78E+9
87.60	2536.27	115.82E+9

$$\left.\begin{array}{c} \delta_{fore-aft}(x)=\int_0^{L_t}\left(\int_0^{L_t}\left(\int_0^{L_t}\frac{1\times dx}{EI(x)}\right)dx\right)dx \\ \delta_{fore-aft}(L_t)=0;\ \frac{d\delta_{fore-aft}(L_t)}{dx}=0 \\ \frac{d^2\delta_{fore-aft}(0)}{dx^2}=0 \end{array}\right\} \Rightarrow K_2=\frac{1}{\delta_{fore-aft}(0)}. \tag{8}$$

Box I

s_{12}=9.6527e-05, s_2=0.1165, and $\tilde{s}_2$=4.1225. The damping ratio of the tower of the wind turbine is considered equal to 0.1% [27]; however, this value changes with the blades' pitch angle changes. Also, the damping of the MIT/NREL TLP is about 0.01%, and the damping of the MIT/NREL TLP is frequency dependent [28]. Therefore, the parameters b_1 and b_2 are assigned as 6.1449e-04 and 0.0053, respectively.

The wave and wind-induced forces are calculated via FAST V8.0. The FAST output, LSShftFxa, the rotor thrust force, is equal to the wind-induced force. FAST calculates the wind-induced force via Aerodyn code, in which the Blade Element Momentum theory is used to calculate the wind-induced forces [29]. Likewise, the FAST output HydroFxi equals the hydrodynamic forces exerted on the platform. The Hydrodyne code is implemented in the FAST to calculate the wave induced forces. The wave-induced forces are calculated using the potential flow theory and Morison's equation [26].

The simulations are carried out in case of a steady uniform wind profile and irregular waves (white noise) with a significant wave height of 8 m. A power-law wind profile is used in FAST code to generate a steady uniform wind profile with a reference speed of 20 $\frac{\text{m}}{\text{s}}$ in a reference height of 90 m with a power-law exponent equal to 0.2 [30]. The corresponding Fast Fourier Transform (FFT) of the exerted forces due to the irregular waves, as well as the uniform wind, are depicted in Figures 4 and 5. The Root Mean Square (RMS) values of the exerted wave and wind forces are 1.8×10^4 N and 210×10^3 N. As shown in

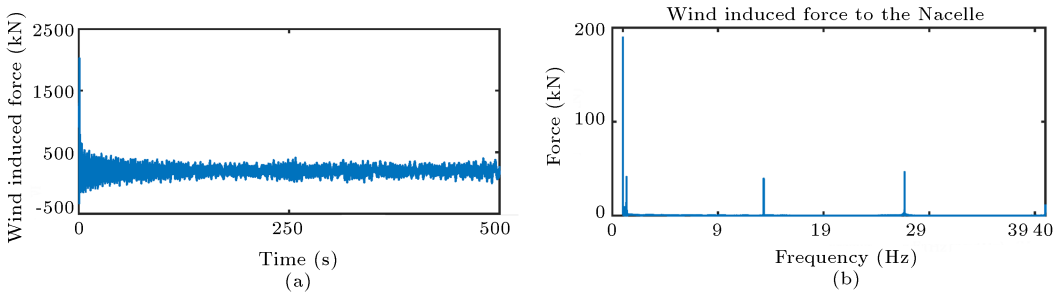

Figure 4. (a) Wind-induced force and (b) corresponding FFT.

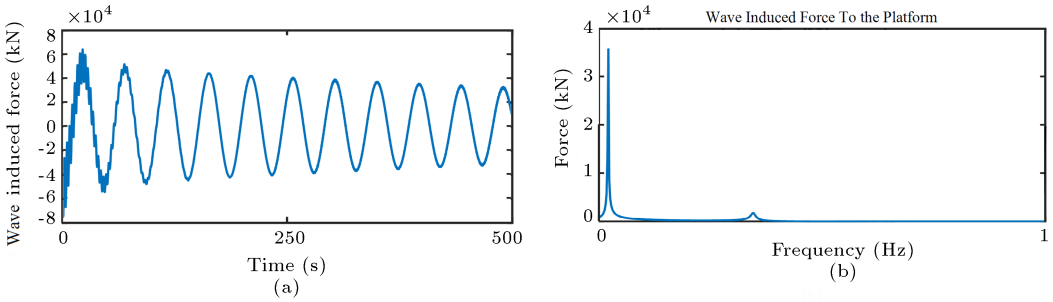

Figure 5. (a) Wave-induced force and (b) corresponding FFT.

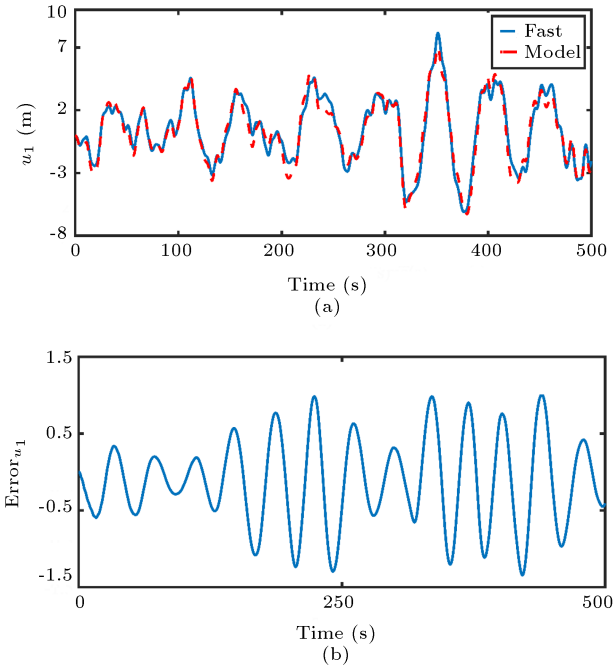

Figure 6. (a) Comparison of the time history of the surge displacements of the FAST and proposed model and (b) corresponding error of the proposed model.

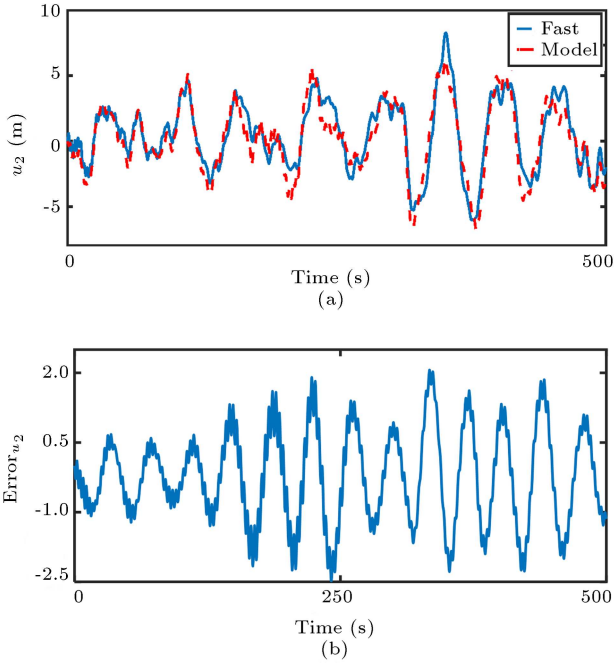

Figure 7. (a) Comparison of the time history of the tower tip displacements of the FAST and proposed model and (b) corresponding error of the proposed model.

Figure 4(b), the frequency corresponding to the max wind-induced force is approximately zero. However, there are some significant amplitudes corresponding to the approximately 0.3, 13.3, and 26 Hz frequencies. Similarly, the wave-induced force is depicted in Figure 5(a). According to Figure 5(b), the wave induced-force approximately has a frequency band between 0 and 0.4 Hz. However, the dominant frequency of the wave-induced force is about 0.15 Hz. According to the above discussions, the wind and wave loading on the floating wind turbine structure may vary in frequencies and amplitudes based on the operational conditions of the floating wind turbine, ranging from uniform winds to hurricanes.

Time domain simulations are carried out by applying the wind and the wave forces obtained by the FAST code to Eq. (7). Results of the simulations and their comparison with the results of the FAST code are shown in Figures 6 and 7. In Figures 6 and 7(a), the time history of the surge displacements of the FAST (solid blue line) and proposed model (red dashed line) are plotted. The difference between the FAST code and the proposed model is calculated by subtracting them, and as it is observed, the proposed model has good accuracy in predicting the surge motions of the platform. However, according to Figure 7, the proposed model does not predict the tower tip displacements as accurately as the surge motion while still having satisfactory accuracy as a conceptual model.

3. Approximate analytical solution by perturbation method and its analysis

In order to analyze the equations of the motion of the floating wind turbine, the MTS method will be employed. The MTS method is one of the strongest and most recognized perturbation methods for analyzing nonlinear systems [31]. In this section, the MTS

method is employed to study the nonlinear dynamics of the floating wind turbine. Thus, the approximate solution of Eq. (7) could be expressed as:

$$u_1(t) = u_{11}(T_0.T_1) + \epsilon u_{12}(T_0.T_1) + \dots,$$

$$u_2(t) = u_{21}(T_0.T_1) + \epsilon u_{22}(T_0.T_1) + \dots, \quad (9)$$

where the T_0 and $T_1 = \epsilon T_0$ represent the fast and slow time scales, respectively. For the time derivatives with respect to time, one has:

$$\frac{\partial}{\partial t} = D_0 + \epsilon D_1 + \dots,$$

$$\frac{\partial}{\partial t^2} = D_0 + 2\epsilon D_0 D_1 + \cdots,$$

$$\text{where} \quad D_k = \frac{\partial}{\partial T_k}, \quad k = 1, 2. \quad (10)$$

To ensure that the coupling factors, forces, and damping terms appear in the same order, Eq. (7) is rewritten as:

$$\ddot{u}_1 + s_{11}u_1 + \epsilon s_{12}u_1^3 - \epsilon s_2 u_2 + \epsilon b_1 \dot{u}_1 = \epsilon f_{wave},$$

$$\ddot{u}_2 + \tilde{s}_2 u_2 - \epsilon \tilde{s}_2 u_1 + \epsilon b_2 \dot{u}_2 = \epsilon f_{wind}. \quad (11)$$

By substituting Eqs. (9) and (10) and rearranging the equation according to the like powers of ϵ, one has:

$$O(\epsilon^0):$$

$$D_0^2 u_{11} + s_{11}u_{11} = 0,$$

$$D_0^2 u_{21} + \tilde{s}_2 u_{21} = 0, \quad (12)$$

$$O(\epsilon^1):$$

$$D_0^2 u_{12} + s_{11}u_{12} = -2D_0 D_1 u_{11} - D_0 u_{11} b_1 + s_2 u_{21} - s_{12}u_{11}^3 + f_{wave}\cos(\Omega_1 T_0),$$

$$D_0^2 u_{22} + \tilde{s}_2 u_{22} = -2D_0 D_1 u_{21} - D_0 u_{21} b_2 + \tilde{s}_2 u_{11} + f_{wind}\cos(\Omega_2 T_0). \quad (13)$$

The general solution of Eq. (13) is:

$$\begin{cases} u_{11} = A_1(T_1)e^{i\omega_1 T_0} + \bar{A}_1(T_1)e^{-i\omega_1 T_0} \\ u_{22} = A_2(T_1)e^{i\omega_2 T_0} + \bar{A}_2(T_1)e^{-i\omega_2 T_0} \end{cases} \quad (14)$$

where $\omega_1 = \sqrt{s_{11}}$, $\omega_2 = \sqrt{\tilde{s}_2}$, and $A_1(T_1)$ and $A_2(T_1)$ are the complex amplitudes of the surge and tower tip vibrations, respectively.

By substituting Eq. (14) into Eq. (13), we have:

$$D_0^2 u_{12} + \omega_1^2 u_{12} = -A_1^3 s_{12} e^{3iT_0\omega_1} - 3A_1^2 \bar{A}_1 s_{12} e^{iT_0\omega_1} + A_2 s_2 e^{iT_0\omega_2} + \frac{1}{2} f_{wave} e^{iT_0\Omega_1} - 2iD_1 A_1 \omega_1 e^{iT_0\omega_1} - iA_1 b_1 e^{iT_0\omega_1} + cc, \quad (15)$$

$$D_0^2 u_{22} + \omega_1^2 u_{22} = A_1 \tilde{s}_2 e^{iT_0\omega_1} + \frac{1}{2} f_{wind} e^{iT_0\Omega_2} - iA_2 b_2 e^{T_0\omega_2} - 2ie^{iT_0\omega_2}\omega_2 D_1 A_2 + cc. \quad (16)$$

Here, cc stands for the complex conjugate of the previous terms.

3.1. Non-resonance vibrations of the FOWT

In the non-resonant case, according to the solvability condition, the secular terms involving $e^{T_0\omega_1}$ and $e^{T_0\omega_2}$ should be equal to zero in order to calculate the periodic solution [31]. Therefore, the solvability condition yields:

$$-iA_1 b_1 \omega_1 - 3A_1^2 s_{12}\bar{A}_1 - 2i\omega_1 D_1 A_1 = 0, \quad (17)$$

$$-iA_2 b_2 - 2i\omega_2 D_1 A_2 = 0. \quad (18)$$

In order to solve the above equations, the A_1 and A_2 are rewritten in the polar form as follows:

$$A_n = \frac{1}{2} a_n e^{i\phi_n} \qquad i = 1, 2. \quad (19)$$

By substitution of Eq. (17) into Eqs. (15) and (16) and separating the real and imaginary parts, we have:

$$-\frac{1}{2} b_1 \omega_1 a_1 - \omega_1 \dot{a}_1 = 0,$$

$$-\frac{3}{8} s_{12} a_1^3 + \omega_1 a_1 \dot{\phi}_1 = 0,$$

$$-\frac{1}{2} b_2 \omega_2 a_2 - \omega_2 \dot{a}_2 = 0,$$

$$-\frac{1}{2} b_2 \omega_2 a_2 - \omega_2 \dot{a}_2 = 0,$$

$$\omega_2 a_2 \dot{\phi}_2 = 0. \quad (20)$$

The solution for the a_1 and a_2, which are the amplitudes of the A_1 and A_2, is as follows:

$$a_n = a_{n0} e^{-\frac{1}{2} b_n \omega_n T_0}. \quad (21)$$

According to Eq. (18), the amplitudes of vibration decay over time, representing a typical solution for damped vibrations under non-resonant conditions.

3.2. Internal resonance vibrations of the FOWT

The internal resonance occurs in the free oscillations of the multi-degrees of freedom systems, which leads to complex nonlinear responses. Internal resonance is most frequent in systems with commensurable frequencies. The natural frequency of the surge motion of the platform and that of the tower fore-aft vibrations are considerably different, but the systems' natural frequency may alter due to the failures and growing fatigue cracks [32]. Nevertheless, according to Eqs. (15) and (16), the 1:1 internal resonance may occur in the floating wind turbine when $\omega_1 \approx \omega_2$, then we have:

$$\omega_2 = \omega_1 + \epsilon\sigma_1, \tag{22}$$

where σ_1 is the detuning parameter, used to express the proximity of the system to resonance conditions. By substituting Eq. (22) into Eqs. (15) and (16), under the internal resonance conditions, the solvability condition yields:

$$e^{iT_1\sigma_1} s_2 A_2 - iA_1 b_1\omega_1 - 3A_1^2 s_{12}\bar{A}_1 - 2i\omega_1 D_1 A_1 = 0, \tag{23}$$

$$e^{-iT_1\sigma_1} A_1\tilde{s}_2 - iA_2 b_2 - 2i\omega_2 D_1 A_2 = 0. \tag{24}$$

Same as the previous section, Eq. (21) is substituted in the above equation, that after separating the real and imaginary parts, one has:

$$\begin{aligned}
&\frac{1}{2}b_1\omega_1 a_1 + \frac{1}{2}\sin\left(T_1\sigma_1 - \phi_1 + \phi_2\right) s_2 a_2 - \omega_1\dot{a}_1 = 0,\\
&-\frac{3}{8}s_{12}a_1^3 + \frac{1}{2}\cos\left(T_1\sigma_1 - \phi_1 + \phi_2\right) s_2 a_2 + \omega_1 a_1\dot{\phi}_1 = 0,\\
&-\frac{1}{2}\sin\left(T_1\sigma_1 - \phi_1 + \phi_2\right)\tilde{s}_2 a_1 - \frac{1}{2}b_2\omega_2 a_2 - \omega_2\dot{a}_2 = 0,\\
&\frac{1}{2}\cos\left(T_1\sigma_1 - \phi_1 + \phi_2\right)\tilde{s}_2 a_1 + \omega_2 a_2\dot{\phi}_2 = 0.
\end{aligned} \tag{25}$$

3.3. Vibrations of the FOWT turbine under the combination of primary and internal resonances

The floating wind turbines are prone to the primary resonance due to the stochastic broadband loadings of the wind and the wave, as shown in Figures 4 and 5. These forces increase the possibility of the primary resonance, which may be coupled with the internal resonance. Therefore, to study the primary resonance condition accompanying the internal resonance condition, in the Case I, we have:

$$\begin{aligned}
&\omega_2 = \omega_1 + \epsilon\sigma_1,\\
&\Omega_1 = \omega_1 + \epsilon\sigma_2,
\end{aligned} \tag{26}$$

where σ_1 and σ_2 are the detuning parameters. After substituting Eq. (26) into Eqs. (15) and (16), the solvability condition yields:

$$\begin{aligned}
&\frac{1}{2}b_1\omega_1 a_1 + \frac{1}{2}\sin\left(T_1\sigma_1 - \phi_1 + \phi_2\right) s_2 a_2\\
&\qquad + \frac{1}{2}\sin\left(T_1\sigma_1 - \phi_1\right) f_{wave} - \omega_1\dot{a}_1 = 0,\\
&-\frac{1}{8\omega_1 a_1}\big(-4\cos(\gamma_1) f_{wave} - 8\sigma_2\omega_1 a_1 + 3s_{12}a_1^3\\
&\qquad - 4\cos\left(\gamma_2\right) s_2 a_2\big) = \dot{\gamma}_1,\\
&-\frac{1}{2}\sin\left(T_1\sigma_1 - \phi_1 + \phi_2\right)\tilde{s}_2 a_1 - \frac{1}{2}b_2\omega_2 a_2 - \omega_2\dot{a}_2 = 0,\\
&\frac{1}{2}\cos\left(\gamma_2\right)\tilde{s}_2 a_1 - \sigma_1\omega_2 a_2 + \sigma_2\omega_2 a_2,
\end{aligned} \tag{27}$$

where $\gamma_1 = T_1\sigma_2 - \phi_1$ and $\gamma_2 = T_1\sigma_1 + \phi_1 - \phi_2$.

In order to study the steady-state response of the system, we should set $\dot{a}_1 = \dot{a}_2 = \dot{\gamma}_1 = \dot{\gamma}_2 = 0$ in Eq. (27), then we have:

$$\begin{aligned}
&-\frac{1}{2}b_1\omega_1 a_1 + \frac{1}{2}\sin\left(\gamma_2\right) s_2 a_2 + \frac{1}{2}\sin\left(\gamma_1\right) f_{wave} = 0,\\
&-\frac{1}{2}\cos(\gamma_1) f_{wave} - \sigma_2\omega_1 a_1 + \frac{3}{8}s_{12}a_1^3 - \frac{1}{2}\\
&\quad \cos\left(\gamma_2\right) s_2 a_2 = 0,\\
&-\frac{1}{2}\sin\left(\gamma_2\right)\tilde{s}_2 a_1 - \frac{1}{2}b_2\omega_2 a_2 = 0,\\
&\frac{1}{2}\cos\left(\gamma_2\right)\tilde{s}_2 a_1 - \sigma_1\omega_2 a_2 + \sigma_2\omega_2 a_2 = 0,
\end{aligned} \tag{28}$$

where γ_1 and γ_2 could be eliminated by the algebraic manipulations; therefore, we have the frequency equation of Case I as:

$$\left(\frac{\left(\frac{1}{2}b_1\omega_1 a_1\right)^2 - \frac{1}{2}\left(-\frac{b_2\omega_1 a_2}{\tilde{s}_2 a_1}\right) s_2 a_2}{f_{wave}}\right)^2 + \left(\frac{\frac{\frac{1}{2}(\sigma_1\omega_2 a_2 - \sigma_2\omega_2 a_2)}{\frac{1}{2}\tilde{s}_2 a_1} + \sigma_2\omega_1 a_1 - \frac{3}{8}s_{12}a_1^3}{f_{wave}}\right)^2 = 1,$$

$$a_2^2\frac{\left(b_2\omega_2\right)^2 + \left(\sigma_1\omega_2 - \sigma_2\omega_2\right)^2}{\tilde{s}_2^2} - a_1^2 = 0. \tag{29}$$

In the Case II of the combination of the primary resonance and internal resonance, we have:

$$\begin{aligned}
&\omega_2 = \omega_1 + \epsilon\sigma_1,\\
&\Omega_2 = \omega_2 + \epsilon\sigma_2,
\end{aligned} \tag{30}$$

where σ_1 and σ_2 are the detuning parameters. After substituting Eq. (30) into Eqs. (15) and (16), the solvability condition yields:

$$\frac{1}{2}b_1\omega_1 a_1 + \frac{1}{2}\sin(\gamma_2)\, s_2 a_2 - \omega_1 \dot{a}_1 = 0,$$

$$\sigma_1\omega_1 a_1 + \sigma_2\omega_1 a_1 - \frac{3}{8}s_{12}a_1^3 + \frac{1}{2}\cos(\gamma_2)\, s_3 a_2 - \omega_1 a_1\dot{\gamma}_1 - \omega_1 a_1\dot{\gamma}_2 = 0,$$

$$\frac{1}{2}\sin(\gamma_1)f_{wind} - \frac{1}{2}\sin(\gamma_2)\tilde{s}_2 a_1 - \frac{1}{2}b_2\omega_2 a_2 - \omega_2\dot{a}_2 = 0,$$

$$\frac{1}{2}\cos(\gamma_1)\, f_{wind} + \frac{1}{2}\cos(\gamma_2)\,\tilde{s}_2 a_1 + \sigma_2\omega_2 a_2 - \omega_2 a_2\dot{\gamma}_1 = 0, \quad (31)$$

where $\gamma_1 = T_1\sigma_2 - \phi_2$ and $\gamma_2 = T_1\sigma_1 - \phi_1 + \phi_2$.

To study the steady-state response of the system, we should set $\dot{a}_1 = \dot{a}_2 = \dot{\gamma}_1 = \dot{\gamma}_2 = 0$ in Eq. (31), which yields:

$$\frac{1}{2}b_1\omega_1 a_1 + \frac{1}{2}\sin(\gamma_2)\, s_2 a_2 = 0,$$

$$\sigma_1\omega_1 a_1 + \sigma_2\omega_1 a_1 - \frac{3}{8}s_{12}a_1^3 + \frac{1}{2}\cos(\gamma_2)\, s_3 a_2 = 0,$$

$$\frac{1}{2}\sin(\gamma_1)\, f_{wind} - \frac{1}{2}\sin(\gamma_2)\,\tilde{s}_2 a_1 - \frac{1}{2}b_2\omega_2 a_2 = 0,$$

$$\frac{1}{2}\cos(\gamma_1)\, f_{wind} + \frac{1}{2}\cos(\gamma_2)\,\tilde{s}_2 a_1 + \sigma_2\omega_2 a_2 = 0. \quad (32)$$

γ_1 and γ_2 could be eliminated by algebraic manipulations; therefore, we have the frequency equation of the Case II as:

$$\left(\frac{\left(\left(\frac{-b_1\omega_1 a_1}{s_2 a_2}\right)\tilde{s}_2 a_1\right)^2 + b_2\omega_2 a_2}{f_{wind}}\right)^2 + \left(\frac{-\frac{\left(\frac{3}{4}s_{12}a_1^3 - 2(\sigma_1\omega_1 a_1 + \sigma_2\omega_1 a_1)\right)}{2s_3 a_2}\tilde{s}_2 a_1 - \sigma_2\omega_2 a_2}{f_{wind}}\right)^2 = 1,$$

$$\left(\frac{-b_1\omega_1 a_1}{s_2 a_2}\right)^2 + \left(\frac{\left(\frac{3}{4}s_{12}a_1^3 - 2(\sigma_1\omega_1 a_1 + \sigma_2\omega_1 a_1)\right)}{s_3 a_2}\right)^2 = 1. \quad (33)$$

4. Simulations of the realistic problem, results, and discussion

In this section, the accuracy of the approximate analytic solution of the method of MTS and the stability of the system in discussed resonance cases are investigated. The time history of the governing equations of the motion of the floating wind turbine

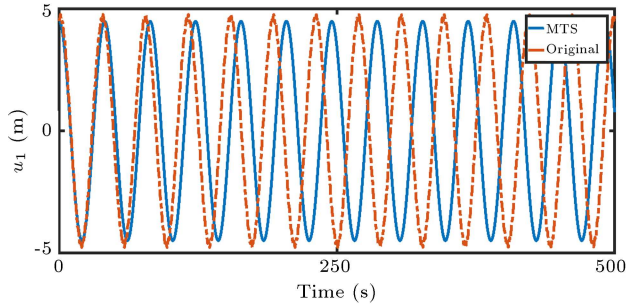

Figure 8. Comparison of the time history of the surge displacement predicted by the approximate solution and the original solution.

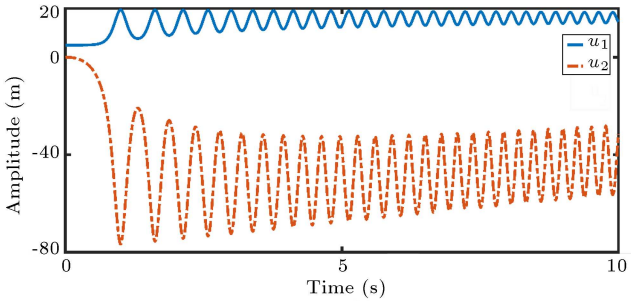

Figure 9. Free vibration amplitude of the floating wind turbine in case of internal resonance.

and the first approximate solution obtained by the method of MTS, which is obtained in the preceding section, is shown in Figure 8. The error of the approximate solution increases with the time; however, the accuracy is satisfactory and acceptable. This accuracy is especially good for predicting the amplitude of the surge vibrations, while the frequencies of time signals have a minor difference. It should be noted that only the first approximate solution of MTS is considered. If the higher approximate solutions are also included in the method, more accurate responses can be obtained. On the other hand, the inclusion of the higher approximate solutions makes the analysis more complex in real conditions.

4.1. Internal resonance conditions

The time history of the free oscillations of the floating wind turbine in the case of the internal resonance as well as $\sigma_1 = 0.001$ is depicted in Figure 9. As it is shown, the time history of the amplitude of the surge motion and that of the tower tip fore-aft motion are oscillatory and obviously, the energy transfer exists between the modes of the vibrations. It should be noted that due to the presence of damping, these vibrations are damped over time (while, at the same time, energy is transferred between the two mentioned modes).

Accordingly, any means that cause the natural frequency of the TLP in the surge direction and the natural frequency of the tower of the wind turbine in

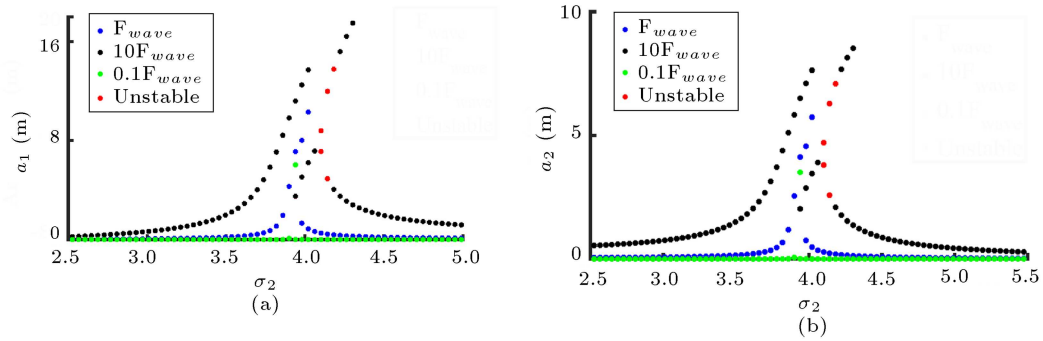

Figure 10. Frequency response curve in case of primary and the internal response due to the wave loading for various amplitude of excitations ($F_{wave} = 1.8e4$, $10F_{wave} = 1.8e5$, $0.1F_{wave} = 1.8e3$, $K_{12} = 1.74e3$, and $d_1 = 1.105e4$) for (a) surge and (b) tower tip fore-aft vibrations.

the transverse direction to get close may lead to internal resonance with a considerable amplitude, which may cause catastrophic events. Growing cracks in the tower structure, the addition of vibration absorbers to the structure, and mis designed mooring systems of the TLP may affect the natural frequencies of both the TLP and the tower.

4.2. Combination of the internal and primary resonance

According to the frequency equations, Eqs. (29) and (33), a trivial solution and nontrivial solution exist for the a_1 and a_2 in case of the resonance in the wave and wind loadings. In the trivial case, both a_1 and a_2 are zero, and in the nontrivial case, both of them are nonzero. The effects of the main parameters, such as the amplitude of the wave loading, wind loading, nonlinear stiffness k_{12}, and platform damping, on the combination of internal and primary resonance amplitudes, are investigated. The stability of the response is investigated via the eigenvalue problem of the coefficient matrix of Eqs. (28) and (32) to determine the stability of the steady-state motions. In this regard, the Jacobin matrix of the corresponding equation should be written as follows:

$$\begin{bmatrix} \frac{\partial f_1}{\partial a_1} & \frac{\partial f_1}{\partial a_2} & \frac{\partial f_1}{\partial \gamma_1} & \frac{\partial f_1}{\partial \gamma_2} \\ \frac{\partial f_2}{\partial a_1} & \frac{\partial f_2}{\partial a_2} & \frac{\partial f_2}{\partial \gamma_1} & \frac{\partial f_2}{\partial \gamma_2} \\ \frac{\partial f_3}{\partial a_1} & \frac{\partial f_3}{\partial a_2} & \frac{\partial f_3}{\partial \gamma_1} & \frac{\partial f_3}{\partial \gamma_2} \\ \frac{\partial f_4}{\partial a_1} & \frac{\partial f_4}{\partial a_2} & \frac{\partial f_4}{\partial \gamma_1} & \frac{\partial f_4}{\partial \gamma_2} \end{bmatrix}. \tag{34}$$

Then, the eigenvalue problem of each point should be calculated. If the corresponding eigenvalues have negative real parts, the steady motion is stable; otherwise, it is unstable. In this regard, the frequency curves are plotted for the platform surge vibrations and the tower tip fore-aft vibrations according to the various wind and wave loadings, several amounts of the platform damping, as well as nonlinear stiffnesses concerning the variations in detuning parameters σ_2 and σ_1.

According to Figure 10, the amplitude of the vibrations is increases with the amplitude of the wave loading. Obviously, as the amplitude of the loading increases, instabilities, jumps, and bifurcations occur in the results. As is seen from the figures, as the amplitude of the wave loadings increases for the different values of the detuning parameter, σ_2, sometimes more than one solution exists. For wave loadings equal to $10F_{wave}$, for the $3.931 \leq \sigma_2 \leq 4.061$, there exist two stable results, one of which corresponds to the $a_2 = 0$. For the $4.141 \leq \sigma_2 \leq 4.182$, there exist two results, one of which is unstable. Accordingly, any means that leads to the increase in the exerted wave load in the surge direction will increase the nonlinearity of the dynamic of the offshore wind turbine, which may lead to devastating consequences. For example, the miss-design of the floating part of the TLP or the mis-implementation of the FOWT and hurricanes may impose large forces in the surge direction. The effect of the damping coefficient d_1 is investigated in Figure 11. As expected, as the damping coefficient is increased, the amplitude of the vibrations is decreased. Accordingly, redesigning the floating platform to increase damping caused by the interaction between fluid and solid is recommended. The amplitude of the steady vibrations for the several values of nonlinear stiffness k_{12} is shown in Figure 12. As the value of the nonlinear stiffness is increased, steady results tend to behave similar to Duffing-type oscillators. In some cases, for certain values of the detuning parameters, three results may exist, with one corresponding to internal resonances where $a_1 = 0$ and $a_2 \neq 0$. Therefore, an increase in the extensional stiffness, i.e., AE, or a decrease in the length of the mooring lines L or any circumstance that increases the amplitude of the surge vibrations, will increase nonlinear stiffness and lead to nonlinear phenomena such as jump and bifurcation and other instabilities. Similarly, in the case of the wind loading, the amplitude of the steady vibrations are illustrated in Figure 13,

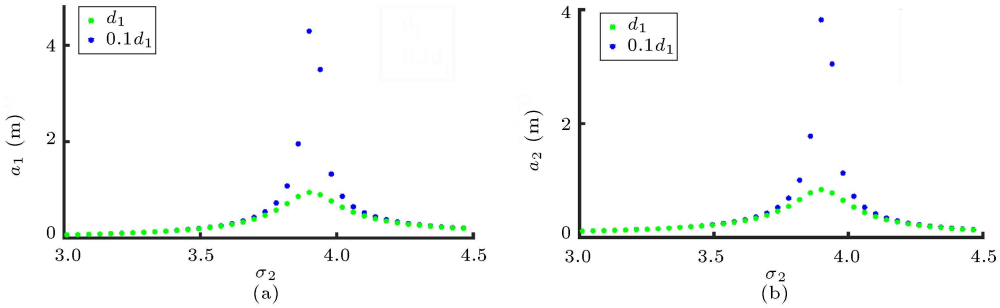

Figure 11. Frequency response curve in case of primary and the internal response due to the wave loading for various damping d_1 values ($F_{wave} = 1.8e4$, $K_{12} = 1.74e3$, $d_1 = 1.105e4$, and $0.1d_1 = 1.105e3$) for (a) surge and (b) tower tip fore-aft vibrations.

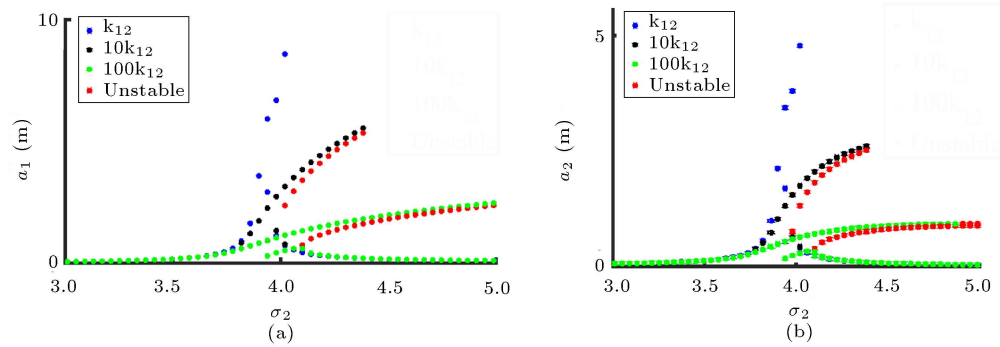

Figure 12. Frequency response curve in case of primary and the internal response due to the wave loading for various nonlinear stiffness k_{12} values ($F_{wave} = 1.8e4$, $K_{12} = 1.74e3$, $10K_{12} = 1.74e4$, $100K_{12} = 1.74e4$, and $d_1 = 1.105e4$) for (a) surge and (b) tower tip fore-aft vibrations.

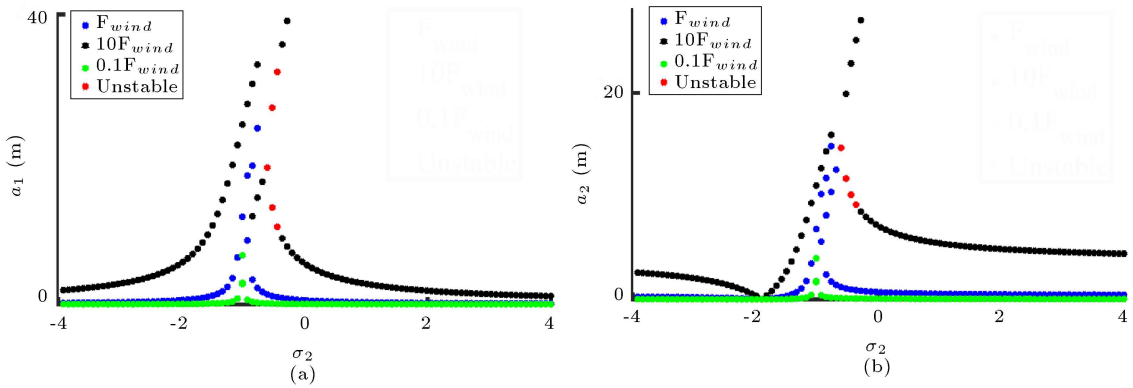

Figure 13. Frequency response curve in case of primary and the internal response due to the wind loading for various amplitude of excitations ($F_{wind} = 210e3$, $10F_{wind} = 210e4$, $0.1F_{wind} = 210e2$, $K_{12} = 1.74e3$, and $d_1 = 1.105e4$) for (a) surge and (b) tower tip fore-aft vibrations.

Figures 14, and 15 for the several wind loadings, damping parameters d_1, and nonlinear stiffness k_{12}, respectively, concerning the variation of the detuning parameters σ_2. Similar phenomena with respect to the previous case of wave loading are observed in the case of wind loading, as the wind loading amplitude, damping coefficient, and nonlinear stiffness vary. In Figure 13 as the amplitude of the wave loading increases, the vibrations' amplitude increases as well. The nonlinear phenomena such as jump and the unstable periodic solution appear as the amplitude of the wind force increases in case of $10F_{wind}$. For $-0.848 \leq \sigma_2 \leq -0.68$ there are two stable solutions, one of which corresponds to the internal resonance where $a_1 = 0$ and $a_2 \neq 0$. As expected, In Figure 14, it is shown the bigger damping coefficient decreases the amplitude of the oscillations. Figure 15 depicts the effect of the several values of the k_{12} on the amplitude of the steady vibrations in the case of wind loading. According to Figure 15, as the value of the k_{12} increased, the nonlinearity in the

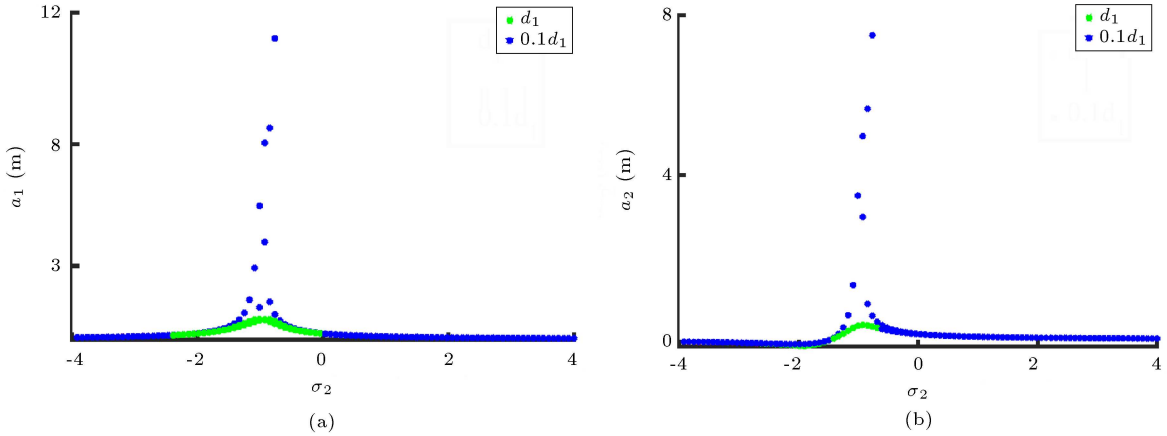

Figure 14. Frequency response curve in case of primary and the internal response due to the wind loading for various amplitude of excitations ($F_{wind} = 210e3$, $K_{12} = 1.74e3$, $d_1 = 1.105e4$, and $0.1d_1 = 1.105e3$) for (a) surge and (b) tower tip fore-aft vibrations.

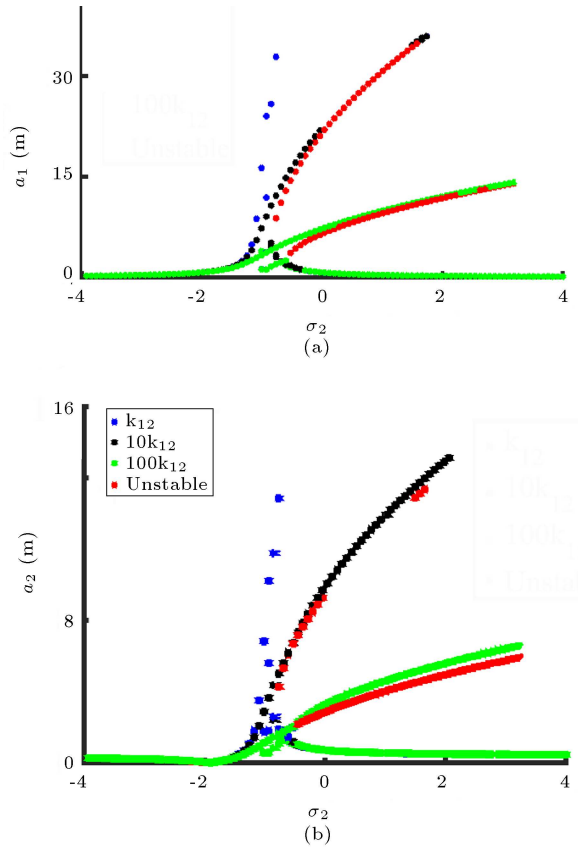

Figure 15. Frequency response curve in case of primary and the internal response due to the wind loading for various amplitude of excitations ($F_{wind} = 210e3$, $K_{12} = 1.74e3$, $10K_{12} = 1.74e4$, $100K_{12} = 1.74e4$, and $d_1 = 1.105e4$) for (a) surge and (b) tower tip fore-aft vibrations.

frequency response got stronger, and jump phenomena became more severe as well. For case $10k_{12}$, for the detuning parameter $-0.7677 \leq \sigma_2 \leq -0.9292$, there are two stable solutions, one of which corresponds to the internal resonance where $a_1 = 0$ and $a_2 \neq 0$.

5. Conclusions

The transverse vibrations of the floating wind turbine mounted on the Tension Leg Platform (TLP) are investigated in this paper. First, a simple conceptual model for the transverse dynamics of the floating wind turbine is driven, in which the degrees of freedom for platform surge motions and tower tip displacements are taken into account. The equivalent stiffness of the platform surge motion and the tower tip fore-aft is then calculated. The suggested model's vibration time history is compared to the vibration time history calculated using the FAST code to validate the model.

The perturbation method is used to explore internal resonance phenomena and how they interact with primary resonance. The relationship between the steady motion amplitudes in the case of internal resonance is derived in this regard. Additionally, by plotting the frequency curves, it is explored how the resonance vibrations' amplitudes are affected by wave and wind loadings, nonlinear stiffness, and platform damping. According to the results obtained, the following remarks can be extracted:

- The phenomenon of internal resonance was studied, and oscillatory results were observed, in which the energy transfer occurs between degrees of freedom;
- Any means that cause the natural frequency of the TLP in the surge direction and the natural frequency of the transfer vibrations of the tower of the wind turbine to get closer may lead to the occurrence of internal resonance that has considerable amplitude. Growing cracks in the structure of the tower, adding vibration absorbers to the structure, and misdesigning the mooring system of the TLP may affect the natural frequency of the TLP as well as the tower;
- The platform surge vibrations and the fore-and-aft

vibrations of the tower both increase as the wind and wave excitations' amplitudes rise;

- As the amplitudes of wind and wave excitation rise, nonlinear phenomena such as unstable oscillations, jumps, and bifurcations occur. As can be seen from the figures, there may be more than one solution as the amplitudes of wave loadings increase for various values of the detuning parameter, σ_2. Therefore, any method that increases the wind or wave load exerted in the direction of the surge will amplify the nonlinear dynamics of the offshore wind turbine, potentially leading to disastrous effects;
- The floating platform's damping ratio has a considerable impact on reducing the fore-and-aft vibrations of the tower and the surge vibrations of the platform. As a result, it is advised to adjust the floating platform so that it has a higher damping ratio;
- Any situation that increases the amplitude of surge vibrations, such as a decrease in the length of the mooring lines or an increase in extensional stiffness, AE, increases the amount of nonlinear stiffness, which in turn increases the nonlinearity of the structure and causes harmful nonlinear phenomena like jump and bifurcation.

Acknowledgment

The authors acknowledge the "Research Office of Sharif University of Technology, Tehran, Iran" for supporting this research through the grant program #QA010910.

Nomenclature

u_1	Surge displacement
u_2	Tower tip displacement (transverse)
K_1	TLP stiffness in surge direction
K_2	Tower stiffness in surge direction
T_0	pretension in tendons in intact condition
ΔT	Change in pretension in tendons
M_{tower}	Mass of the tower
M_{added}	Added mass
l	Elevation from bottom of the tower
F_{wave}	Wave exerted load
E	Module of elasticity
A	Area of cross section
L	Tendon length
K_0	Extensional stiffness of the tendons $(\frac{A_{tendon}E_{tendon}}{L})$
K_{11}	$4\frac{T_0}{L}$
K_{12}	$4\frac{\mathrm{AE}}{2\mathrm{L}^3}{u_1}^2$
M_1	Mass of the platform
d_1	Equivalent damping coefficient of the platform
d_2	Damping coefficient of the wind turbine tower
$E_{tower}I_{tower}$	Tower fore-aft stiffness (N.m^2)
$\rho_{tower}A_{tower}$	Mass density (kg.m)
F_{wind}	Wind exerted load
ρ	Density
I	Moment of inertia

References

1. Ren, Z., Verma, A.S., Li, Y., et al. "Offshore wind turbine operations and maintenance: A state-of-the-art review", *Renewable and Sustainable Energy Reviews*, **144**, 110886 (2021). DOI:10.1016/j.rser.2021.110886
2. Collu, M. and Borg, M. "Design of floating offshore wind turbines", In *Offshore Wind Farms*, Elsevier, pp. 359–385 (2016). DOI:10.1016/B978-0-08-100779-2.00011-8
3. Mas-Soler, J., Uzunoglu, E., Bulian, G., et al. "An experimental study on transporting a free-float capable tension leg platform for a 10 MW wind turbine in waves", *Renewable Energy*, **179**, pp. 2158–2173 (2021). DOI:10.1016/j.renene.2021.08.009
4. Jain, A.K., "Nonlinear coupled response of offshore tension leg platforms to regular wave forces", *Ocean Engineering*, **24**(7), pp. 577–592 (1997).
5. Senjanović, I., Tomić, M., and Rudan, S. "Investigation of nonlinear restoring stiffness in dynamic analysis of tension leg platforms", *Engineering Structures*, **56**, pp. 117–125 (2013). DOI:10.1016/j.engstruct.2013.04.020
6. Tabeshpour, M.R., Ahmadi, A., and Malayjerdi, E. "Investigation of TLP behavior under tendon damage", *Ocean Engineering*, **156**, pp. 580–595 (2018).
7. Walia, D., Schünemann, P., Hartmann, H., et al. "Numerical and physical modeling of a tension-leg platform for offshore wind turbines", *Energies*, **14**(12), p. 3554 (2021).
8. Wang, J., Luo, Y., Wang, Y., et al. "Dynamic response of tension leg platform with hydro-pneumatic tensioner under second-order waves and freak waves", *Ocean Engineering*, **252**, p. 111261 (2022).
9. Tabeshpour, M.R. and Hedayatpour, R. "Analytical investigation of nonlinear heave-coupled response of tension leg platform", *Proceedings of the Institution of Mechanical Engineers, Part M: Journal of Engineering for the Maritime Environment*, **233**(3), pp. 699–713 (2019). DOI:10.1177/1475090218776430
10. Jonkman, J.M., *Dynamics Modeling and Loads Analysis of an Offshore Floating Wind Turbine*, University of Colorado at Boulder (2007).

11. Tagliafierro, B., Karimirad, M., Martınez-Estévez, I., et al. "Numerical assessment of a tension-leg platform wind turbine in intermediate water using the smoothed particle hydrodynamics method", *Energies*, **15**(11), p. 3993 (2022). DOI:10.3390/en15113993

12. Tabeshpour, M.R. and Nikmehr, L. "Numerical and experimental study on dynamic response mitigation of tension leg platform using tuned mass damper", *Journal of Ship Research*, **66**(4), pp. 265–276 (2021).

13. Dai, S.S., Chaplin, J.R., Younis, B.A., et al. "Computations and measurements of the global drag force on a tension-leg platform", *Ocean Engineering*, **239**, p. 109710 (2021).

14. Ghabraei, S., Moradi, H., and Vossoughi, G. "Investigation of the effect of the added mass fluctuation and lateral vibration absorbers on the vertical nonlinear vibrations of the offshore wind turbine", *Nonlinear Dynamics*, **103**(2), pp. 1499–1515 (2021). DOI:10.1007/s11071-020-06194-1

15. Keighobadi, J., Mohammadian KhalafAnsar, H., and Naseradinmousavi, P. "Adaptive neural dynamic surface control for uniform energy exploitation of floating wind turbine", *Applied Energy*, **316**, p. 119132 (2022). DOI:10.24200/SCI.2023.61871.7532

16. Jonkman, J.M. and Buhl Jr, M.L., *Fast User's Guide-Updated August 2005*, National Renewable Energy Laboratory (NREL), Golden, CO. (2005).

17. Liu, H.B., Duan, F., Yu, F., et al. "Validation of a FAST spar-type floating wind turbine numerical model with basin test data", *IOP Conference Series: Earth and Environmental Science*, **188**, p. 012096 (2018). DOI:10.1088/1755-1315/188/1/012096

18. Serret, J., Rodriguez, C., Tezdogan, T., et al. "Code comparison of a NREL-FAST model of the levenmouth wind turbine with the GH bladed commissioning results", *Proceedings of the ASME 2018 37th International Conference on Ocean, Offshore and Arctic Engineering*, **10**, pp. 17–22 (2018).

19. Papi, F. and Bianchini, A. "Technical challenges in floating offshore wind turbine upscaling: A critical analysis based on the NREL 5 MW and IEA 15 MW reference turbines", *Renewable and Sustainable Energy Reviews*, **162**, p. 112489 (2022). DOI:10.1016/j.rser.2022.112489

20. Zhu, K. and Chung, J. "Vibration and stability analysis of a simply-supported Rayleigh beam with spinning and axial motions", *Applied Mathematical Modelling*, **66**, pp. 362–382 (2019). DOI:10.1016/j.apm.2018.09.021

21. Esfahani, S., Esmaeilzade Khadem, S., and Ebrahimi Mamaghani, A. "Nonlinear vibration analysis of an electrostatic functionally graded nano-resonator with surface effects based on nonlocal strain gradient theory", *International Journal of Mechanical Sciences*, **151**, pp. 508–522 (2019). DOI:10.1016/j.ijmecsci.2018.11.030

22. Lackner, M.A. "Controlling platform motions and reducing blade loads for floating wind turbines", *Wind Engineering*, **33**(6), pp. 541–553 (2009). DOI:10.1260/0309-524X.33.6.541

23. Adilah, A. and Iijima, K. "A spectral approach for efficient fatigue damage evaluation of floating support structure for offshore wind turbine taking account of aerodynamic coupling effects", *Journal of Marine Science and Technology*, **27**(1), pp. 408–421 (2021). DOI:10.1007/s00773-021-00841-x

24. Pan, Q., Mahfouz, M.Y., and Lemmer, F. "Assessment of mooring configurations for the IEA 15MW floating offshore wind turbine", *Journal of Physics: Conference Series*, **2018**(1), p. 012030 (2021). DOI:10.1088/1742-6596/2018/1/012030

25. Jonkman, J.M. and Matha, D. "Dynamics of offshore floating wind turbines-analysis of three concepts", *Wind Energy*, **14**(4), pp. 557–569 (2011).

26. Jonkman, J., Robertson, A., and Hayman, G. "Hydro dyn user's guide and theory manual, NREL, 2014", *Available online. Assessed on Dec* (2014).

27. Jonkman, J., Butterfield, S., Musial, W., et al. *Definition of a 5-MW Reference Wind Turbine for Offshore System Development*, National Renewable Energy Lab. (NREL), Golden, CO. (United States) (2009). DOI:10.2172/947422

28. Matha, D., *Model Development and Loads Analysis of an Offshore Wind Turbine on a Tension Leg Platform with a Comparison to Other Floating Turbine Concepts*: April 2009, National Renewable Energy Laboratory (NREL), Golden, CO. (2010). DOI:10.2172/973961

29. Jonkman, J., Hayman, G., Jonkman, B., et al. "Aerodyn v15 user's guide and theory manual", *NREL: Golden*, CO., USA (2015).

30. Platt, A., Jonkman, B., and Jonkman, J. "Inflowwind users guide", *Technical Report* (2016).

31. Nayfeh, A.H. and Mook, D.T., *Nonlinear Oscillations*, John Wiley & Sons (2008).

32. Prawin, J. and Rao, A.R.M. "Nonlinear structural damage detection based on adaptive volterra filter model", *International Journal of Structural Stability and Dynamics*, **18**(02), p. 1871003 (2018).

Biographies

Soheil Ghabraei received the BSc and MSc degrees in Mechanical Engineering from the Sharif University of Technology in 2013 and 2015, respectively. He is currently pursuing a PhD degree at the Department of Mechanical Engineering, Sharif University of Technology. His current research interests include system dynamics and nonlinear vibration.

Hamed Moradi received a BSc, Mechanical Engineering degree in solid mechanics from Amirkabir

University of Technology in 2005; MSc and PhD Mech. Eng. in applied mechanics from Sharif University of Technology (SUT), Tehran, Iran, in 2008 and 2012. Currently, he is an Associate Professor in the Department of Mechanical Engineering at Sharif University of Technology. His current research interests include the modeling of dynamic systems and the application of robust, nonlinear, and optimal control methods in various dynamic systems such as manufacturing, bioengineering, thermo-fluid industrial processes, renewable energy, and power plant engineering.

Gholamreza Vossoughi received his PhD from the Mechanical Engineering Dept. at the University of Minnesota in 1992. Ever since he has been a faculty member of the Mechanical Engineering Dept. at the Sharif University of Technology. He served as the Manufacturing Engineering and Applied Mechanics Division Director from 1994 to 1998 and as the Graduate Dean of Mechanical Engineering from 1999–2003.